World Scientific Research Journal (WSRJ) ISSN: 2472-3703
www.wsr-j.org

Analysis of Microstructure and Residual Stress of 316L Weldment

Yicheng Yang [1, a], Fuwei Lv [2, b], Zehua Liang [3, c], Jiangui Sun [3, d]

[1]Chemical process machinery, Shandong University of Science and Technology, Qingdao, China.

[2]Power Engineering, Shandong University of Science and Technology, Qingdao, China.

[3]Mechanical Manufacturing and Automation, Shandong University of Science and Technology, Qingdao, China.

[a]1450851002@qq.com,[b]673716592@qq.com,[c]972492713@qq.com,

[d]sunjiangui123@163.com

Abstract: The secondary development of finite element simulation software ABAQUS and FORTAN language was used to simulate the TIG welding process of 316L and the residual stress field after welding. The welding process was simulated by indirect coupling of temperature field and stress field. The FORTAN language implements the loading of mobile heat sources and the "live and dead cell" bead filler. The results of the temperature field over time are obtained, and the residual stress of the entire welded joint is analyzed against the stress field. It is concluded that the residual stress of the entire welded joint is symmetrical about the weld, and the maximum transverse residual stress appears at the center of the weld at the weld. The position of the welding foot is approximately 5 mm from the center of the weld. And with the position away from the center of the weld, the stress value has a significant downward trend. The difference between the simulated value and the experimental value is small.

Keywords: 316L, welding residual stress, finite element simulation.

---

1. INTRODUCTION

As an ultra-low carbon austenitic stainless steel, 316L has been widely used at home and abroad. The reason why this kind of steel can be favored by most people is that its cold-rolled products have good appearance glossiness, excellent resistance to pitting corrosion, strong work hardening and non-magnetic properties in the solution state, and most importantly, 316L has excellent high-temperature strength and is therefore widely used as a welding material in pipelines, heat exchangers and chemical industries [1].This article mainly uses 316L austenitic

stainless steel plate as the research object. By using finite element analysis software such as ABAQUS [2] and finite element analysis method as the main theory, the 316L steel plate model is established in the simulation analysis, and the experiment is required by ABAQUS software. Some of 316L's physicochemical properties were added to the model that was created, and fine mesh finite element meshing was performed on the model. By setting different properties, analysis steps, interactions and loads, the temperature field and stress field simulation experiments are respectively set. In this paper, the double ellipsoidal heat source model theory was used to simulate the welding process of two welding seams in the welding process using the Fortran language [3], in order to analyze the thermal conditions and stress conditions of the 316L steel plate under dynamic heat source.

2. SAMPLE PREPARATION AND TEST METHODS

2.1 Pample preparation

The material to be welded is 316L stainless steel. The chemical composition is shown in Table 1. The size of 316L steel plate is 100mm×100mm×6mm. Two butt weldings are performed using argon gas shielded welding. The one-side open 45° groove is covered by electric welding. The back is not open groove, leaving 1-2mm gap argon arc welding, as shown in Figure 1.

When welding 316L stainless steel, it is not possible to use welding rods of type A302. A302 welding rods are welding consumables of austenitic stainless steels and strength-type low-alloy steels, that is, welding consumables of dissimilar steels such as 304 or 316 and 10, 20, and Q245R. Therefore, this experiment used 316L brand ER316L electrode. Its chemical composition is shown in Table 2 [4].

Table 1. 316L element content

chemical composition	C	Si	Mn	P	S	Ni	Cr	Mo
content (%)	<=0.03	<=1.00	<=2.00	<=0.035	<=0.03	10.0-14.0	16.0-18.0	2.0-3.0

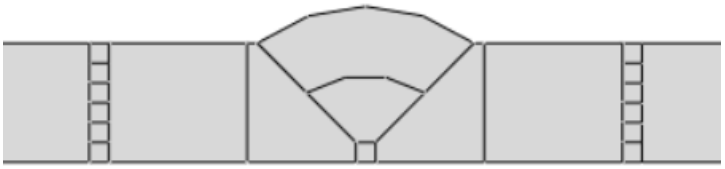

Figure 1 316L docking diagram

Table 2. Chemical composition of ER316L electrode (wt.%)

Grade	C	Si	Mn	S	P	Cr	Ni	Mo
ER316L	0.03	0.60	1.86	0.008	0.015	18.00	12.00	2.3

In the welding process, a certain current needs to be applied to the steel plate. Experimental data is shown in Table 3 below.

Table 3. Welding process parameters of two welding

First pass	Electric current /A	Voltage /V	Second pass	Electric current /A	Voltage /V
1	120	10	2	80	11

The time required for the first pass is 50.00 s, and the time required for the second pass is 59.88 s. This results in a first welding speed of 0.002 m/s and a second welding speed of 0.00167 m/s.

2.2 Test methods

In this experiment, an X-ray stress tester of type X-350A was used. The X-ray method [5] is generally limited to test the residual stress of the surface layer for the test size of the steel. At present, the use of electrochemical corrosion stripping to measure the residual stress is a more general method. However, electrochemical corrosion stripping is used to measure the residual stress, but the methods generally used are short-time and small-area methods. The device used is for thinner components and the corrosion surface is smaller. And due to corrosion conditions, corrosion time, corrosion power, corrosive media and other factors. So it is prone to excessive corrosion.

3. METALLOGRAPHIC OBSERVATIONS

In 316L, the highest content is austenite, and the austenitic microstructure is shown in Figure 2.

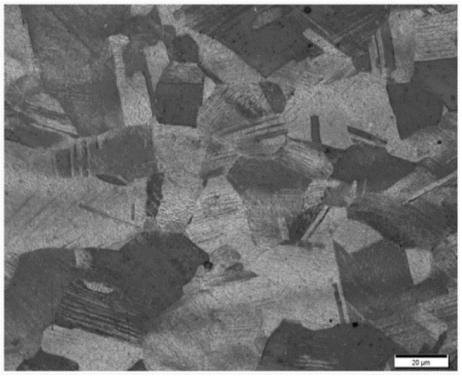

Figure 2. Austenite metallographic structure

Sample analysis was performed on the 316L base metal. The austenite structure is generally an irregular large-grained polygonal grain, crystal grain boundaries are clearly visible, and no other second phase is mixed. As shown in Figure 3. Austenite metallographic analysis of heat affected zones at different locations is shown in Figures 4, and 5. The weld joint is composed of three parts: heat affected zone, fusion line and weld. Generally, grain coarsening in the heat affected zone deteriorates the plastic toughness of the material and becomes one of the weak links in the welded structure.

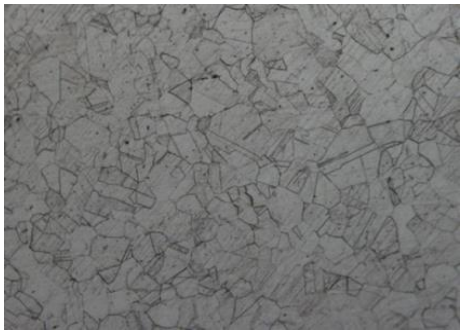

Figure 3. 316L metallographic 200 times

From the topography of the 316L welded joint, the microstructure can be clearly divided into three areas: welding top, welding, and welding bottom. These three parts contain the basic features of the entire fusion line. From the metallography, the weld line is clearly visible both at the top, middle and root of the weld. The parent metal near the fusion line is also a isochronal austenite grain. The size and the austenite grain size of the parent metal in the distance are somewhat different. The grain near the fusion line increases and the volume is coarsened. Although no spheroids were formed, there were obvious slip lines inside the grains. The slip line has a high degree of parallelism and can be determined as a lattice slip band [6].

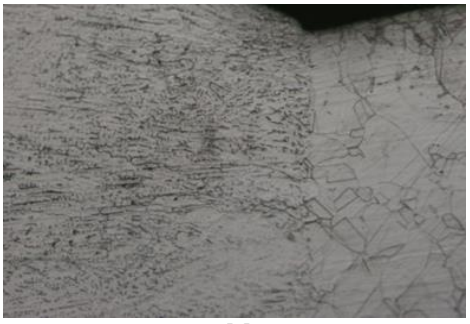

Figure 4. Joint welding top 200 times

Figure 5. Joint welding 200 times

4. FINITE ELEMENT MODEL ESTABLISHMENT

4.1 Grid division

In the process of model meshing, the meshes at the welds are encrypted, and the heat affected zone and the welds are used in an area of 10 mm to 12 mm in the over-grid area, and the base metal area is sparse. The model cell uses an eight-node linear heat transfer hexahedral element DC3D8 with a total number of elements of 26301. The mesh model is shown in Figure 6.

4.2 Material parameters

The thermodynamic performance parameters of 316L steel change with the effect of the welding heat source, and its size is shown in Table 3.2.

Consider the Q345R latent heat of 300,000 J/kg, the solidus temperature of 1420° C, and the liquidus temperature of 1460° C.

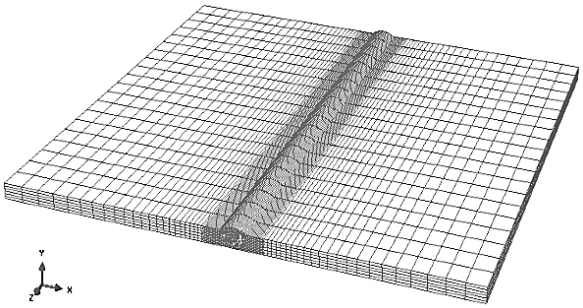

Figure 6. 316L three-dimensional finite element model

Table 4. 316L thermodynamic performance parameters table

temperature (℃)	20	200	400	600	800	1000	1200
Heat transfer (W /(m×K))	13.31	16.33	19.74	22.38	25.07	27.53	29.76
density (kg / m3)	7966	7893	7814	7724	7630	7535	7436
Specific heat capacity (J /(kg ×K))	470	508	550	592	634	676	719

4.3 Boundary conditions and loads

All surfaces of the plate were selected to convert to a convection heat transfer surface, the absolute zero was -273.15° C, and the initial temperature before welding was 20° C. Thermal radiation [7] and thermal convection are the main methods for heat exchange between the welding and the environment, in which the emissivity is 0.85, the Stefan-Boltzmann constant is 5.67W/m2 • K4, and the convection heat transfer coefficient is 10W mK. The load is the body heat flux acting on both welds, and its size is 1.

5. SIMULATION RESULTS AND TEST VERIFICATION

5.1 Temperature field simulation analysis

In this paper, a sequential coupling analysis method and process are adopted for the numerical simulation of 316L stainless steel plate welding. Therefore, the accurate temperature field obtained by the simulation is an important prerequisite for the analysis of the subsequent welding stress field. At the same time, the temperature field distribution rule directly to the stress strain field. The distribution has an effect. Here, the temperature field results are analyzed and displayed first.

As shown in Fig.7-10, the temperature field simulation results for t=0, 0.1944s, 3.558s, 25.84s, and 57.34s were extracted, respectively, and the results were analyzed in chronological order.

It can be seen from the figure that at the beginning of the welding, the weld was not filled with material at first, then the filler material was added first, and then the welding heat source was applied at the moment when the welding heat source first appeared. The welding heat source

can be considered as the moving distance is small, then the temperature field is similar to the fixed heat source, and the temperature gradient is in the form of several concentric circles centered on the welding heat source, and the temperature outward gradually decreases from the center of the heat source. As shown in Figure 8.

FIG.9 is a temperature field distribution cloud diagram when the first lane is welded to 25.84. It can be seen that the temperature distribution has reached the quasi-steady-state stage and continues to advance in the welding direction regularly until the end of this pass. The weld zone is rapidly heated and melted, and the velocity is much higher than in the surrounding area. At the same time, it is accompanied by strong thermal convection and radiation, resulting in a large thermal gradient, and the temperature on both sides of the weld is basically symmetrical. This is due to the slower heat transfer of the austenitic stainless steel and the obvious result of the large gap between the welding heat source temperature and the plate temperature. The unwelded areas are densely distributed with temperature gradients with minimal spacing. The actual situation where the compound is rapidly heated. The welded area is cooled by natural radiation, the temperature gradient changes smoothly, the spacing is large, and the actual condition of the composite weldment cooling. Therefore, the isotherm of the bead surface is symmetrical with an elliptic isotherm. The front is more dense than the rear, and the length of the ellipse is affected by the welding speed. The greater the welding speed, the greater the length, ie, the greater the temperature difference between before and after the heat source. Large, this is an important reason why welding residual stress strain occurs.

FIG. 10 is a cloud distribution of the temperature field at 57.34 s in the first lane. It can be seen that at this time the welding heat source just moved to the end of the weld, the temperature of the weldment is rapidly increased, and will directly affect the residual stress field at the end of the weld.

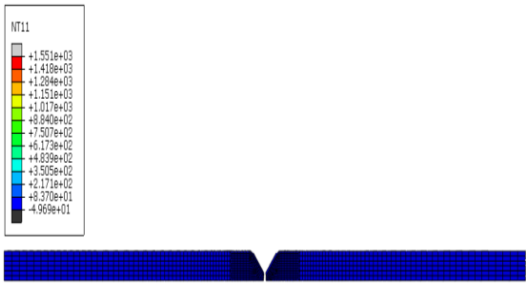

Figure 7. Simulation of temperature field at t=0

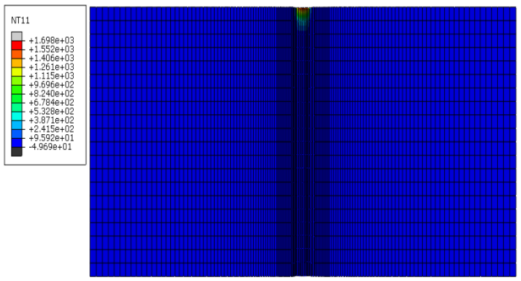

Figure 8. Simulation of temperature field at t=0.1944s

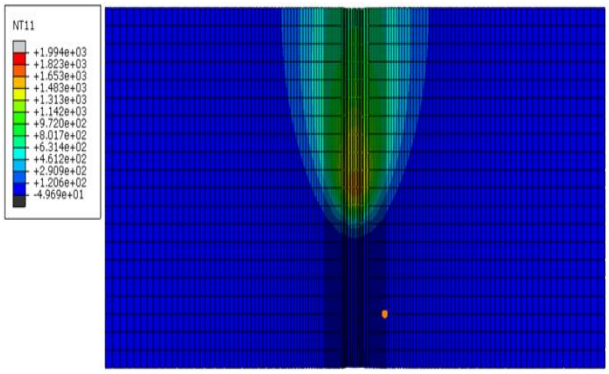

Figure 9. Simulation of temperature field at t=25.84s

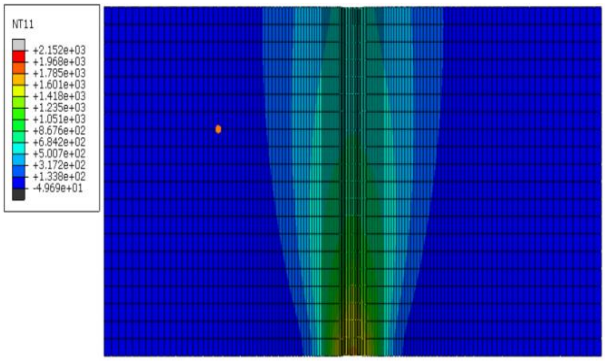

Figure 10. Simulation of temperature field at t=57.34s

Fig. 11-13 is a cloud distribution of the temperature distribution at the end of welding for t = 150, 450s and 2000s. It can be seen that when the welding is completed, the temperature gradient field of the weldment is still centered on the highest temperature and slowly cooled to four weeks, so when t=150s, the weldment is only cooled for 20s. The maximum temperature is 400 ° C. The highest temperature is still at the welding arc. When t=450s, the overall temperature field of the weldment tends to be flat. Basically, with the continuous cooling of the weldment around with the weldment, the high temperature of the weld zone gradually spreads to the base metal, and the temperature decreases slowly. For a weldment with t = 450s, the temperature has dropped to about 160 ° C. As time passes, the maximum temperature gradually decreases and the isotherm range expands accordingly. When the welding is completed, the temperature gradient field of the weldment is still centered on the highest temperature and slowly cooled to four weeks. After the final cooling to room temperature, and the time is 1000 s, the temperature distribution of the steel plate can be seen to be uniform and the center of the steel plate can be seen. The temperature at the weld is the highest, the temperature spreads evenly, and as a result, it falls, reaching the edge where the temperature is lowest, as shown in flg13.

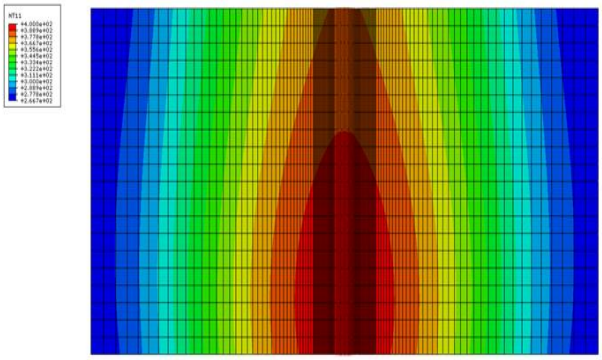

Figure 11. Simulation of temperature field at t=150s

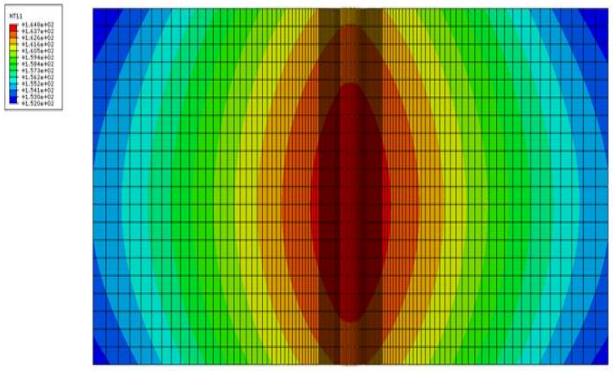

Figure 12. Simulation of temperature field at t=450s

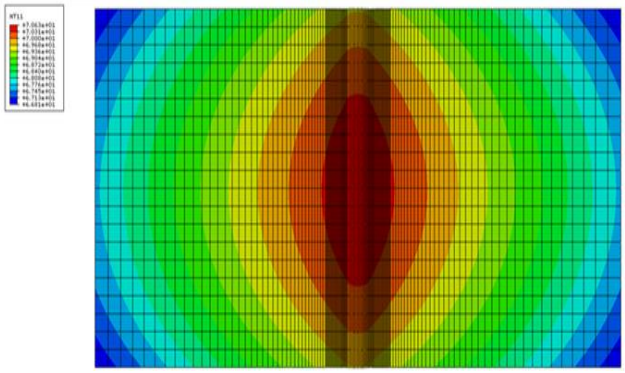

Figure 13. Simulation of temperature field at t=1000s

According to the temperature field, the entire welding temperature field is symmetrically distributed. Therefore, the middle position of the model is selected, and the test points along the straight line path perpendicular to the direction of the weld are selected to read the time-temperature history of the corresponding test points. The time-temperature diagram for each measurement point is shown in Figure 14-17.

The thermal curve with Origin is shown in Figure 15-17 and compared. As the final cooling time is longer and the temperature is significantly lower than 100° C. After cooling to 1000 s, and it is proven that the tendency is to slowly decrease until it is reduced to room temperature. The welding time period is about 200s, so in order to observe the thermal cycle curve more intuitively and clearly, only the temperature value of each point before cooling to 1000s changes with time.

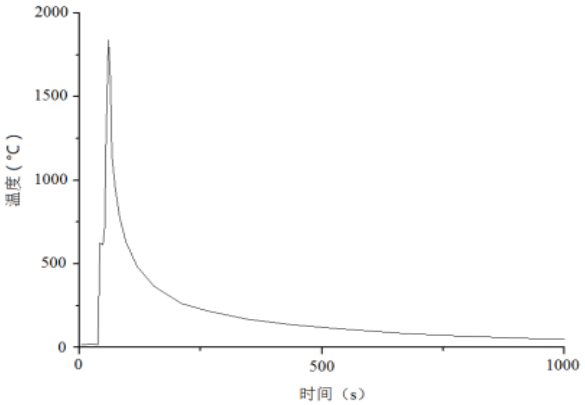

Figure 14. Time-temperature diagram of 1 point welding model

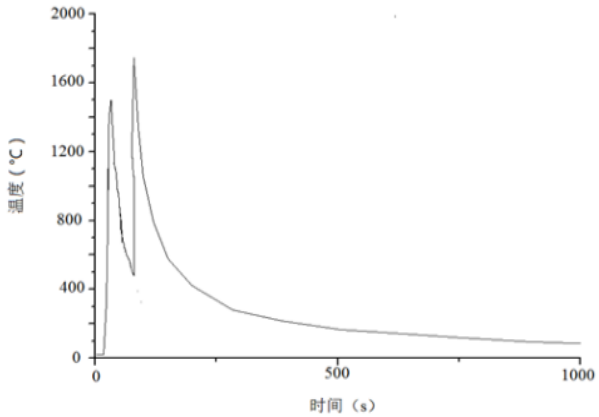

Figure 15. Time-temperature diagram of 2point welding model

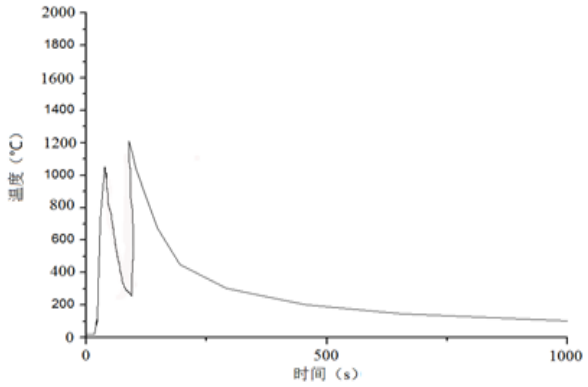

Figure 16. Sketch of 3 point welding time-temperature of welding model

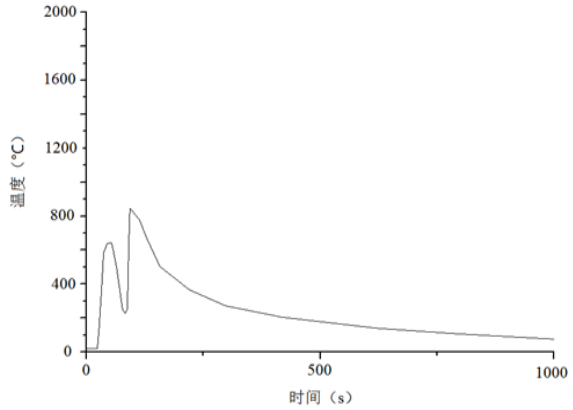

Figure 17. Sketch of 4 point welding time-temperature of welding model

The thermal curve with Origin is shown in Figure 15-16 and compared. As the final cooling time is longer and the temperature is significantly lower than 100° C. after cooling to 1000 s, and it is proven that the tendency is to slowly decrease until it is reduced to room temperature. The welding time period is about 200s, so in order to observe the thermal cycle curve more intuitively and clearly, only the temperature value of each point before cooling to 1000s changes with time.

As can be seen from the figure2 points are the center temperature of theweld surface, and the material was not filled before the first 80 seconds. Therefore, a constant room temperature temperature curve after the start of welding can be observed in the figure, and then 1 temperature is in the second lane. In the welding process, it is affected by the welding heat source, the temperature rises sharply, and the temperature rises to the maximum value. With the end of the weld, 2 o'clock began to cool and a slow decrease in temperature occurred. Comparative observations 1, 3, and 4 are available, because the test point is selected as the center of the welding model, so at the beginning of the temperature rise (that is, when the welding heat source begins to affect), there is a constant room temperature at 0 o'clock from the time point. The time is about 20s or so. This is the time required for the welding heat source to move to the test point. According to the calculation of the welding speed and the length of the weld. Corresponding to the actual situation, and obvious thermal cycling phenomena occur at 2, 3 points, is the temperature rises significantly in a short time, and then slowly decreases according to a certain trend. Then in the second welding, the corresponding temperature curve repeats, the peak value is obvious, and the cooling trend is the same. Therefore, it can be concluded that the formation of a welding thermal cycle.

In the 4 point chart, no obvious peak temperature appears, the temperature change is gentle, and the maximum temperature is low. The change trend of the three-dimensional temperature of the smooth temperature at the beginning of the welding from the above description is basically the same, and is consistent with the actual welding process. The influence of the welding heat source is mainly in the weld seam and its vicinity, and the welding heat cycle is obvious. The highest temperature value in each area is significantly related to the distance from the weld to the area, and there is a certain temperature rise and temperature drop in the area far away from the weld, but the thermal cycle effect is not obvious compared with the weld area.

5.2 Stress field simulation analysis

In stress simulation experiments. The resulting temperature field is added to the stress field to obtain the final residual stress distribution. The residual stress parallel to the direction of the weld is called the longitudinal residual stress, and the stress perpendicular to the direction of the weld is called the transverse residual stress, and the residual stress along the thickness direction is called the thickness residual stress.

From 18-19, it can be seen that in the finally formed stress field, the maximum longitudinal or transverse residual stress occurs in the weld and its surrounding area. This is because the temperature of the weld during welding is the highest, and it is close to the temperature of the welding torch. The temperature of the base metal area far from the weld is low and the residual

stress level is low. In order to simulate a more realistic welding environment, only the four fulcrums of the bottom surface are fully constrained. Therefore, the overall stress distribution is not uniform due to a certain extent, but the stress distribution on the base material areas on both sides of the weld tends to be symmetrical.

From Fig. 19, it can be concluded that there is no uniform variation in the distribution of the isotropic residual stress in the weld zone, but the distribution form is still about the symmetry of the weld on both sides of the base metal region. The transverse residual stress has tensile stress and compressive stress. The two sides of the weldment on the upper and lower surface of the weldment are mainly tensile stress. The intermediate surface of the weld shows tensile stress to compressive stress. The distribution of longitudinal residual stress and transverse residual stress are similar. However, the trend is not the same. There is a significant area of compressive stress farther away from the weld. However, the residual stress in the thickness is relatively low, and there is no obvious change. Therefore, the transverse residual stress is tensile stress and the main stress is in the weld zone. The maximum stress value appears near the upper and lower surface fusion lines.

It can be seen from the figure that the stress is uniformly distributed on the 316L steel plate, the stress is mainly concentrated on the weld, and the stress is evenly reduced near the position of the weld, and the stress does not substantially change at the end of the plate and away from the weld. Only the lateral residual stress is selected as the comparison result. A joint path of 20 mm on the left and right of the upper surface of the weld is selected on the weld model. The corresponding stress values are read as shown in Figure 20 below.

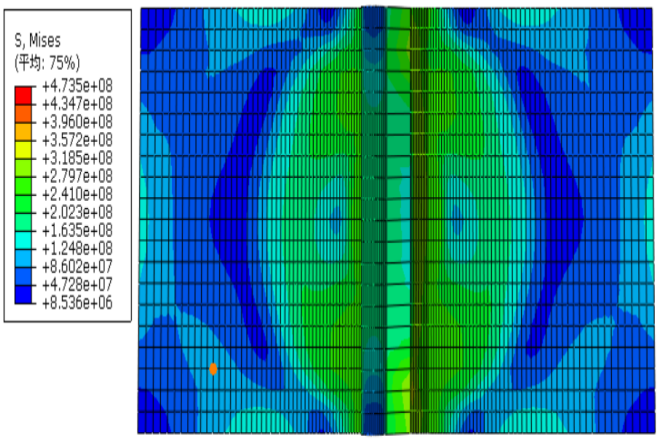

Figure 18. Simulated top view of stress field

As can be seen from Fig. 20, the residual stress at the center of the weld is sharply reduced, and the maximum peak value appears at the center of the weld seam at 5 mm and the maximum peak value is 108.47 MPa. Compare the resulting lateral stress values for the three methods. It can be found that the maximum transverse stress value appears in the left and right of the weld 5mm, that is, the fusion line at the upper surface of the weld, where the solid-liquid boundary point as a weld is subjected to a strong thermal effect in the welding process and cooling process. The force acts so that its force is complex and there are obvious differences between the two tissues.

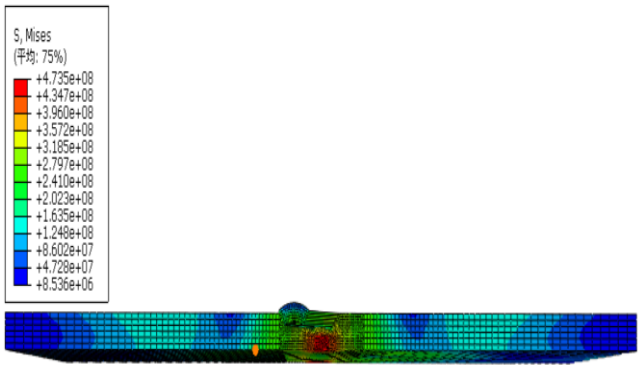

Figure 19. Simulated front view of stress field

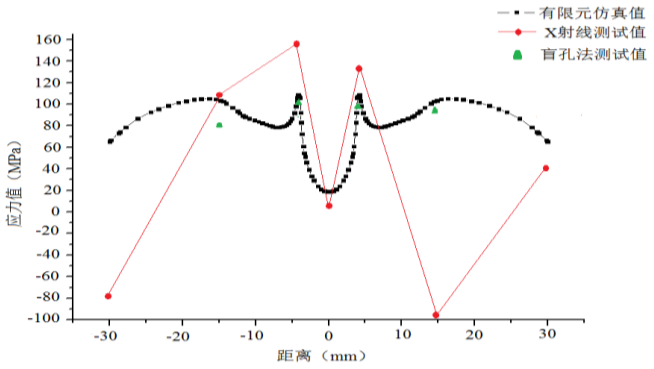

Figure 20. Comparison of results of transverse residual stress in three methods

Table 5. Comparison between simulation results of finite element method and X-ray test method

Position method	1	2	3	4	5	6	7
Finite element method(Mpa)	65.42	100.78	108.47	18.846	108.47	100.78	65.42
X-ray method(Mpa)	-74.60	107.21	160.43	10.55	134.50	-97.03	40.24

The results of the transverse residual stress calculated by the finite element simulation method are in good agreement with those of the other two test results. The results obtained by the X-ray method are in line with the weld area, but the results of the heat affected zone test and the finite element method are quite different. The maximum error is 197.69% and the minimum error is 21.92%. Table5.

6. CONCLUSION

In this paper, the 316L welded joints as the research object, the simulation of 316L welding temperature field and stress field, a total of the following conclusions.

(1) 316L can obtain better welded joints by using TIG welding technology. The overall structure of the welded joints is relatively uniform, with no obvious defects or bubbles, and the overall mechanical properties of the welded joints are good. The weld joints are harder than the welds. In the heat-affected zone on the side, the microstructure of the weld has good anisotropic characteristics. The heat affected zone near the fusion line is significantly affected by the welding heat input. The phenomenon of grain growth is obvious, and there is a clear slip

zone on the surface of the grain. , to prove that the site has undergone a large plastic deformation.

(2) 316L welding in the corresponding welding process to form the welding structure of austenitic and ferritic mixed benign welded joints. The surface of the microstructure has obvious microstructure characteristics. A large number of chromium dendrite axes can be seen in the electron probe at high magnification. The cooling mode of the 316L welded joint in this article is the FA cooling mode. The microstructure of the weld microstructure is similar to that of the heat-affected zone, and there are no significant changes in the left and right sides of the fusion line. No segregation of impurities occurred in the entire weld seam.

(3) The residual stress of 316L welded joints is symmetrically distributed about the welds. The specific distribution of the joints is relatively complex, but the maximum value of the welding residual stress occurs at the weld line of the weld joint. The transverse residual stress of the weld joint is mainly tensile stress and reaches the maximum value at the weld foot. There is a tendency to slowly decrease toward the base metal. The maximum error of X-ray test results and simulation results is 197.69%.

REFERENCES

[1] Mao Nan. Study on microstructure and mechanical properties of 316L stainless steel welded joints [D]. Harbin Institute of Technology, 2012.

[2] Xu Jinquan. Material strength study [M]. Shanghai: Shanghai Jiaotong University Press, 2009.

[3] M. DADFAR.M.H.FATHI, F. KARIMZADEH, M.R. DADFAR, A. SAATCHI.Effect of TIG welding on corrosion behavior of 316L stainless steel [J], Materials Letters 61 (2007) 2343-2346.

[4] SILVACC, MIRANDAHCD, SANT'ANAHBD, et al. Microstructure, hardness and petroleum corrosion evaluation of 316L/AWS E309MoL-16 weld metal [J]. Materials Characterization, 2009, 60(4): 346 – 352.

[5] AHMAD S, MALIK A U. Corrosion Behaviour of Some StainlessSteels in Chlorinated Gulf Seawater [J]. Journal of Applied Electrochemistry, 2001, (31): 1009-1016.

[6] Vaidyanathan S, Todaro A F, Finnie I. Residual due due to circumferential welds [J].Journal of Engineering Materials and Technology, 1973, 95(4): 233-237.

[7] Dong Junhui, Huo Lixing, Zhang Yufeng. Three-dimensional finite element analysis of welding stress and strain of girth welded pipe [J]. Chinese Journal of Mechanical Engineering, 2001, (12):86-90.